Degradation of bentazon herbicide by heterogeneous catalytic ozonation with ZnO-scallop shell nanocomposite: kinetic, reaction pathways and mineralization

Neda Karami[a,b], Azita Mohagheghian[a,b],*, Mehdi Shirzad-Siboni[a,b],*, Kazem Godini[c]

[a]*Research Center of Health and Environment, Guilan University of Medical Sciences, Rasht, Iran,*
Tel. +98 9111309440; email: mohagheghian@yahoo.com (A. Mohagheghian), Tel. +98 9112346428; email: mshirzadsiboni@gums.ac.ir,
mshirzadsiboni@yahoo.com (M. Shirzad-Siboni), Tel. +98 9359572258; email: nedakarami2012@yahoo.com (N. Karami)
[b]*Department of Environmental Health Engineering, School of Health, Guilan University of Medical Sciences, Rasht, Iran*
[c]*Department of Environmental Health Engineering, School of Health, Hamadan University of Medical Sciences, Hamadan, Iran,*
Tel. +98 9188373716; email: kazem_goodyny@yahoo.com

ABSTRACT

In this study, the synthesized ZnO-scallop shell nanocomposite was applied as a catalyst in catalytic ozonation for removal of bentazon from aqueous solutions. Also, the impacts of key parameters (solution pH, catalyst dosage, initial bentazon concentration, oxygen and nitrogen gas, hydrogen peroxide, and organic compounds) on the removal efficiency were studied. It was found that under the optimum conditions: pH = 7, catalyst dose = 0.5 g/L, and initial bentazon concentration = 30 mg/L, the removal efficiency reached 76.86% after 60 min of ozonation; and, in the same conditions, in the presence of 50 mM hydrogen peroxide, the efficiency was 90.47%. Further, the kinetic results showed that the second-order model was more desirable for explaining bentazon degradation. Moreover, under the optimum conditions, the electrical energy per order (E_{EO}) was 102.595 kWh/m^3. In the case of actual drinking water, the removal efficiency of bentazon was 70%, and when synthetic water was tested, 55.56% of the herbicide was mineralized after 60 min. Besides, the reaction pathways of bentazon during ozonation were investigated.

Keywords: Operating parameters; Catalytic ozonation; ZnO-scallop shell; Mineralization; Reaction pathways

1. Introduction

Surface and groundwaters are mainly contaminated with herbicides through leachate, pouring chemicals, runoff from agriculture and herbicide-laden effluents discharged from different industries [1]. The herbicide of bentazon can control the growth of many sedges and broadleaf weeds [2]. The activity of this herbicide is selective and post-emergence. Also, if this herbicide is absorbed through the skin or swallowed, it can carry harmful effects on the body [2]. Eye irritation is also its another effect [2]. In many countries, strict rules have been made for the quality of drinking water due to the destructive effects of pesticides on human health and the environment [3]. According to the World Health Organization (WHO), 0.03 mg/L of bentazon has been accepted as the maximum permissible concentration in drinking water [4]. Also, the WHO has placed bentazon in toxicity Class III [4].

Therefore, water sources and wastewaters containing these herbicides require treatment with an appropriate technology such as adsorption [5–7], photocatalytic degradation [2,8,9], ozonation [10], photo- and electro-Fenton [11], vacuum membrane distillation [12] and oxidation [13]. Advanced

oxidation processes (AOPs) have been developed for the treatment of wastewater, drinking water and industrial effluents; the processes of the photocatalytic, ozonation and Fenton are among these processes [14–16]. Ozone-based AOPs are more attractive than UV-based AOPs for wastewater treatment because turbidity and color in the presence of ozone create less interference for the wastewater treatment process [16]. The catalytic ozonation process (COP) is a new form of AOPs. By adding a catalyst to ozonation, ozone begins to decompose and, in turn, reactive radicals are produced [17]. COPs are both homogeneous and heterogeneous [16]. The higher degradation efficiency and easier separation of the catalyst at the end of the reaction are the benefits of the heterogeneous COPs [18]. Accordingly, this study was carried out to earn materials with appropriate catalytic activities that are also inexpensive and easy for synthesis. Therefore, in order to achieve an active and cheaper catalyst, the ZnO-scallop shell nanocomposite was synthesized. Zinc oxide is used in various industries and its physical properties include conductivity, piezoelectric and magnetism; another important feature of this semiconductor is the broadband saturation energy [19–21]. Scallop shell (marine bivalve) is found abundantly on the shores of the seas and is considered as waste in many restaurants [22].

In this research, we studied the effects of different parameters: solution pH, catalyst dosage, initial bentazon concentration, different purging gases, hydrogen peroxide (H_2O_2) concentration and organic compound type on the removal efficiency of bentazon, by means of the synthesized ZnO-scallop shell nanocomposite. Besides, kinetic study was performed and simulated by the zero, first, second and Langmuir–Hinshelwood kinetic models. And, in order to determine whether the ozone/ZnO-scallop shell process is an economic process or not, the E_{EO} was computed. Also, the degradation rate of bentazon from drinking water was measured. Finally, the reaction pathways and mineralization rate of this herbicide were determined by gas chromatography–mass spectroscopy (GC–MS) and total organic carbon (TOC) analysis.
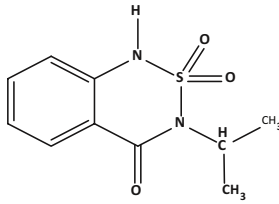
2. Materials and methods

2.1. Chemicals

All of the chemicals used in this study were applied without further purification and were obtained from Merc, Germany. Bentazon (3-isopropyl-1H-2,1,3-benzothiadiazin-4[3H]-one-2,2-dioxide), as a model herbicide, was purchased from Chem-Service (USA). The characteristics of this herbicide have been specified in Table 1.

2.2. Synthesis of ZnO-scallop shell nanocomposites

In this research, scallop shells were collected from the coast of the Caspian Sea in Guilan Province (Iran) and washed several times with distilled water to remove dust. Next, they were dried in the sun. After milling at 1,000°C, they were calcinated for 5 h and graded with American Standard Test Sieve Series (ASTM) 50. The ZnO-scallop shell nanocomposite was synthesized by a co-precipitation method in alkaline conditions [23,24]. Zinc chloride solution ($ZnCl_2$) was obtained by dissolving 13.63 g of zinc chloride in distilled water, the

Table 1
Structure and characteristics of bentazon

Formula	$C_{10}H_{12}N_2O_3S$
λ_{max} (nm)	335
M_w (g/mol)	240.3
Solubility in water (g/L)	0.50

scallop shell powder prepared in the previous step, with a mass ratio of 1:1 (w:w), was added to the zinc chloride solution and then pH of solution was set at 12 using hydroxide sodium. The products in aqueous solution were mixed up for 7 h and then centrifuged and washed with deionized water. Finally, the nanocomposite prepared in oven at 100°C for 3 h was dried.

The method used to determine pH_{pzc} of the ZnO-scallop shell nanocomposite was obtained from the works of other researchers [22,25].

2.3. Characterization instruments

The crystalline structure, functional groups, surface morphology and elemental composition of zinc oxide and ZnO-scallop shell were determined by X-Ray diffractometry (XRD), Fourier-transform infrared spectroscopy (FTIR), scanning electron microscopy (SEM) and energy-dispersive X-Ray spectroscopy (EDX) respectively. All models of these devices have been reported in our previous published article [26]. All ozonation experiments were performed with an ozone generator (model COG-1A, 5 g/h, ARDA, France) in a 1,000-mL ozonation reactor. It should be noted that the ozone dose was fixed at 1.720 mg/min over the experiments. To identify the reaction pathways of bentazon degradation, gas chromatography–mass spectrometry (model Varian GC-MS, USA) was used. In addition, the concentrations of TOC were obtained using a TOC analyzer (model TOC-VCSH, Shimadzu, Kyoto, Japan).

2.4. Experimental procedure and analytical techniques

A stock solution (1,000 mg/L) of bentazon was prepared. In this study, effects of parameters: pH (3, 5, 7, 9 and 11), naonocatalyst dose (0.25, 0.5, 1, 2 and 3 g/L), initial bentazon concentration (10, 20, 30, 40 and 50 mg/L), oxygen and nitrogen gas rate (2 L/min), H_2O_2 concentration (2, 5, 10, 25 and 50 mM) and organic compound type (humic acid, oxalic acid, EDTA, phenol, folic acid and citric acid equal to 30 mg/L) on bentazon degradation by the COP were tested. Also, in the same reaction conditions, for the efficiency of each process: scallop shell, ZnO, ZnO-scallop shell, ozone, ozone-ZnO, ozone/scallop shell and ozone/ZnO-scallop shell were surveyed. Further, under the

optimum conditions, the effect of hydroxyl radical scavenger on bentazon degradation was investigated. The pH of the solutions was adjusted using HCl and NaOH by using a pH meter (Metron, Switzerland). For the catalytic ozonation of bentazon, a solution containing bentazon and the catalyst was made and then 30 min was given to balance; next, the ozonation was carried out for 60 min, and the samples were taken during this time. In order to separate the catalyst from the suspensions, they were centrifuged (Sigma-301, Germany) for 5 min at 4,000 rpm, and then the residual bentazon contents in the suspensions were read by a spectrophotometer device (UV/Vis spectrophotometer, Hach-DR 5000, USA) at λ_{max} = 335 nm [27]. Additionally, kinetic study was performed and simulated by the zero, first, second and Langmuir–Hinshelwood kinetic models. Each experiment was conducted in triplicate, and mean values of data were reported. Because standard deviations never exceeded ±1.5%, the error bars were not shown in the figures. And, in order to determine whether ozone/ZnO-scallop shell is an economic process, the E_{EO} values were computed. Finally, the ability of the ozone/ZnO-scallop process in removing bentazon from drinking water (real water) was studied. Also, the reaction pathways of bentazon degradation during ozonation as well as mineralization rate of bentazon by the COP were determined under the optimum conditions.

3. Results and discussion

3.1. Characterization of the nanocomposite

3.1.1. XRD analysis

The crystal structure of the samples was determined by the XRD patterns (Figs. 1(a) and (b)). The dominant peaks of ZnO depicted as 2θ values are 31.68°, 34.32°, 36.13°, 47.48°, 56.50°, 62.80°, 66.54°, 67.88° and 69.07° corresponding to the (100), (002), (101), (102), (110), (103), (200), (112) and (201) planes of hexagonal wurtzite ZnO (JCPDS card number of 36-1451), respectively, (Fig. 1(a)) [28,29]. After the coating of the ZnO nanoparticles, the peak of zinc oxide was still visible;
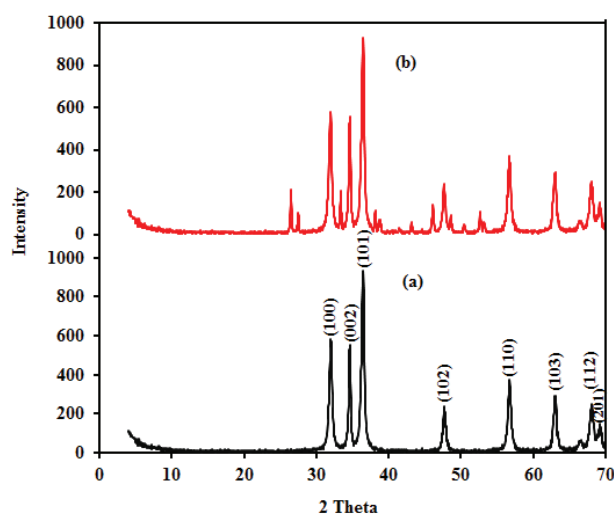
it illustrates that the zinc oxide nanoparticles have grown on the scallop shell (Fig. 1(b)). Using the Debye–Sherrer equation, the average crystallite size of the ZnO-scallop shell nanocomposites was estimated to be about 15 nm.

3.1.2. FTIR analysis

FTIR analysis was performed before and after the coating of ZnO on scallop shell in the range of 400–4,000 cm⁻¹. The active functional groups on the surface of the ZnO nanoparticles and the ZnO-scallop shell nanocomposite have been shown in Figs. 2(a) and (b). The spectrum of this analysis related to the synthesized zinc oxide nanoparticles shows significant absorption peaks at 458, 727, 913 and 3,500 cm⁻¹ (Fig. 2(a)). The band located at 458 cm⁻¹ corresponds to the ZnO nanoparticles; also, this peak is observed in the FTIR patterns of the coated ZnO nanoparticles on scallop shell (Fig. 2(b)). Figs. 2(a) and (b) show a band at 700–900 cm⁻¹, and a band at ~3,500 cm⁻¹ is related to the presence of aromatic C–H stretching and hydroxyl groups, respectively [19].

3.1.3. SEM and EDX analysis

Figs. 3(a)–(c) show the SEM images of the scallop shell, ZnO nanoparticles and scallop shell after the coating of the ZnO nanoparticles. Before coating scallop shell with the ZnO nanoparticles, a flat surface was observed on the scallop shell, which was disappeared due to coating with ZnO. The EDX microanalysis was applied to characterize the elemental of the ZnO nanoparticles and ZnO-scallop shell nanocomposite (Figs. 4(a) and (b)). This analysis determined that weight percentages (wt%) of O and Zn on the zinc oxide nanoparticles were 42.72% and 57.28% and also weight percentages (wt%) of Ca, Zn and O in the ZnO-scallop shell nanocomposite were 16.87%, 34.5% and 45.64%, respectively. Generally, there is a good hybridization between ZnO and scallop shell.

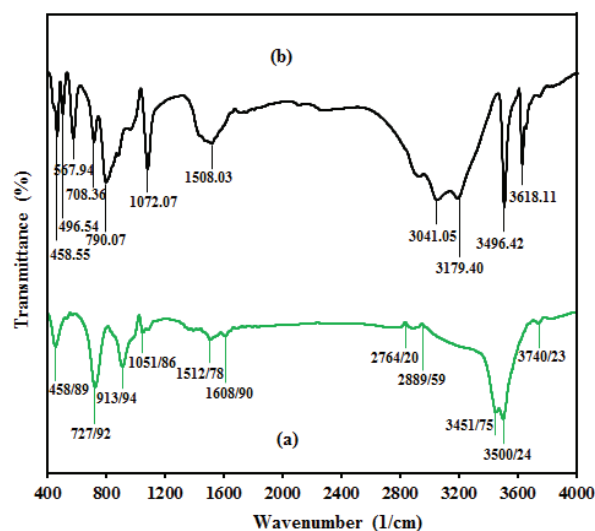Fig. 1. XRD image of the samples: (a) ZnO nanoparticles and (b) ZnO-scallop shell nanocomposite.

Fig. 2. FTIR image of the samples: (a) ZnO nanoparticles and (b) ZnO-scallop shell nanocomposite.
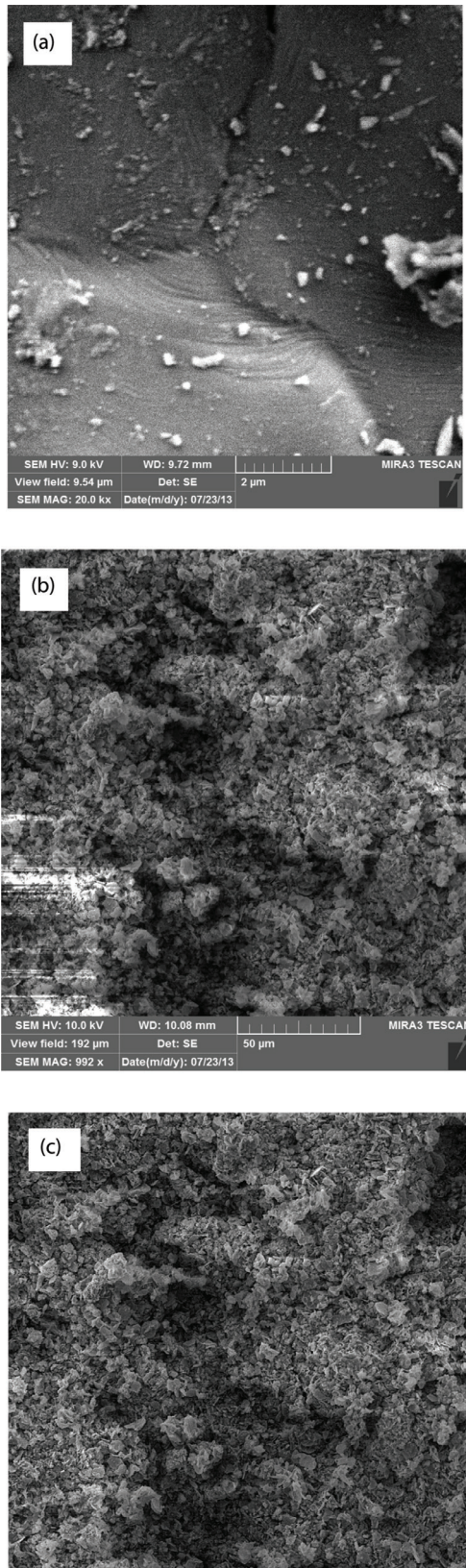
Fig. 3. SEM image of the samples: (a) scallop shell, (b) ZnO nanoparticles and (c) ZnO-scallop shell nanocomposite.

3.2. Effects of different parameters on the removal of bentazon by the COP

3.2.1. Effect of initial pH

The effect of the initial solution pH (3–11) on the degradation of bentazon by the COP was investigated, under the following conditions: initial bentazon concentration (30 mg/L) and catalyst dosage (0.5 g/L) for 60 min (Fig. 5). In this work, when the pH value ranged between 3 and 7 and 9 and 11, the decomposition efficiency increased from 65.17% and 76.86% and almost 75%. Moreover, the pH_{pzc} of the ZnO-scallop shell nanocomposite was found to be approximately 11. And, the pH_{pzc} of zinc oxide and pK_a for bentazon were 9 and 3.3,
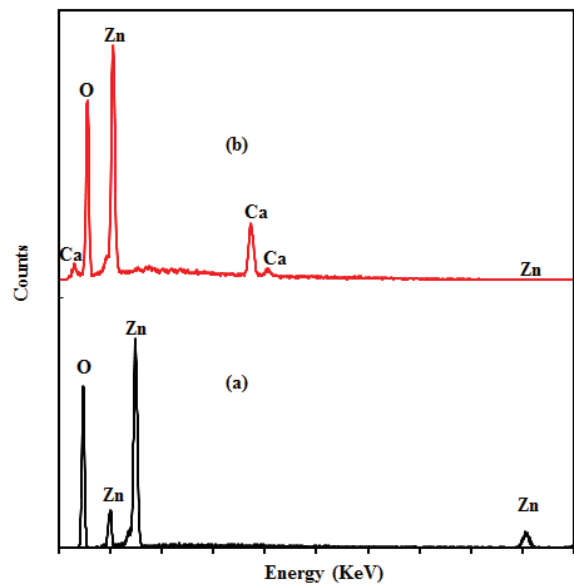

Fig. 4. EDX image of the samples: (a) ZnO nanoparticles and (b) ZnO-scallop shell nanocomposite.
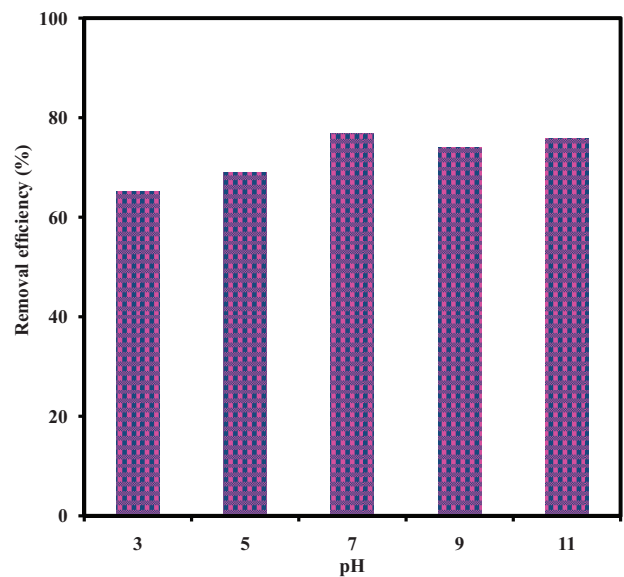

Fig. 5. Effect of initial pH on the degradation of bentazon by the COP (dosage = 0.5 g/L and bentazon concentration = 30 mg/L).

respectively [30,31]. The ZnO-scallop had a positive charge at pHs less than 11. According to electrostatic action and reaction, when the catalyst has a positive charge and pollution has negative charge, they absorb each other. These conditions occur when $pH_a^{Bentazon} < pH < pH_{PZC}^{ZnO\text{-}scallop\ shell}$. Also, there are two methods for destruction of organic pollutants with ozone. The first one is direct oxidation which ozone directly attacks organic pollutants (ozonolysis, electrophilic attack) [31,32]; compounds that have C=C double bonds in their structure and those that have functional groups such as H, CH_3 and OCH_3 are sensitive to ozonolysis [31,33]. It should be noted that, in acidic conditions, the process of direct oxidation occurs [31,34]. The second one is indirect oxidation by which hydroxyl radicals are produced, and these radicals attack organic pollutants. This process happens at alkaline pHs [31].

As stated, the removal of bentazon in neutral conditions was higher than that of alkaline conditions as well as in alkaline conditions higher than acidic conditions. The maximum removal efficiency for bentazon under neutral conditions is probably due to the direct and indirect oxidation of ozone [35–37]. In this study, bentazon removal at pH = 7 was greater than the other pHs studied.

3.2.2. Effect of catalyst dosage

Fig. 6 shows the results of the impact of changing catalyst dosage (0.25–3 g/L) on the degradation of bentazon by the COP, under the following conditions: initial bentazon concentration (30 mg/L) and initial pH (7) for 60 min. With increasing catalyst dosage from 0.25 to 0.5 g/L, the degradation rate increased from 67.87% to 76.86%. And, when the catalyst dosage increased from 1 to 3 g/L, the removal efficiency decreased from 77.06% to 60.47%. The catalyst level and the number of active sites for ozone decomposition increased with increasing catalyst dosage; as a result, the degradation of bentazon increased with increasing dosage [38]. Also, the reduction in efficacy by increasing the dose may be due to the
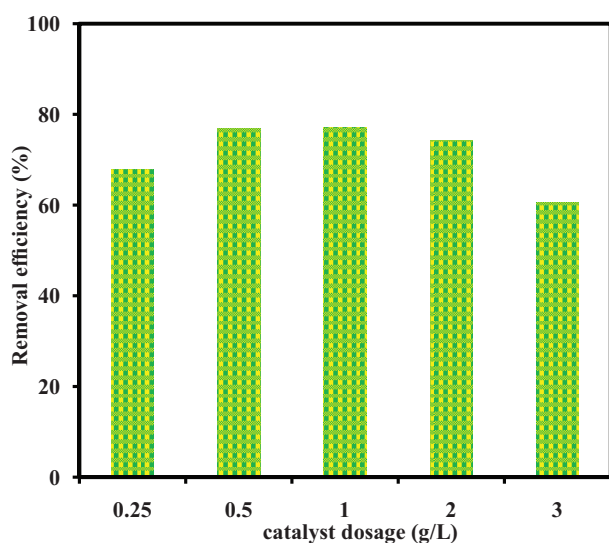
fact that the type of catalysts, contaminant combination, the intended performance level and the reaction conditions for destruction of target pollutants are involved in choosing the optimal catalyst dose for the COP [39,40]. Moreover, catalyst active sites are likely to be closed by increasing the catalyst dose [41]. In this study, bentazon removal at catalyst dosage = 0.5 g/L was more suitable than that at the other doses studied.

3.2.3. Effect of initial bentazon concentration

Effect of initial bentazon concentration on the decomposition rate by the COP was tested by different initial bentazon concentrations (10–50 mg/L), under the following conditions: initial pH = 7, catalyst dosage = 0.5 g/L and contact time = 10–60 min (Fig. 7). The bentazon removal by the COP declined (from 77.38% to 71.21%) when there was an increase in initial bentazon concentration (10–50 mg/L) after 60 min. In this work, an increase in the initial concentration reduced the amount of pollutant oxidation. Other researchers have gained similar results [42]. Accordingly, the more molecules of bentazon in the reactor, the more concentration of by-products there will be [43,44]. Thus, the available ozone should be used to continue the destruction of the original bentazon as well as the oxidation of intermediates [45].

3.2.4. Kinetics and electrical energy per order (E_{EO}) studies

The results of this work were studied with the zero-, first- and second-order equations. The relationship between initial reduction rate (r) and initial bentazon concentration can be described via the Langmuir–Hinshelwood model. The value of E_{EO}, for the destruction of bentazon by the COP, was studied economically. Table 2 shows the formulas for kinetic studies and E_{EO}.

$[Bentazon]_0 - [Bentazon]_t$, $\ln\frac{[Bentazon]_0}{[Bentazon]_t}$ and $\frac{1}{[Bentazon]_t} - \frac{1}{[Bentazon]_0}$ vs. t were calculated to determine the kinetic data to obtain the bentazon degradation rate. Tables 3 and 4 show the kinetic parameters for bentazon degradation models at different

Fig. 6. Effect of initial catalyst dosage on the degradation of bentazon by the COP (pH = 7 and bentazon concentration = 30 mg/L).
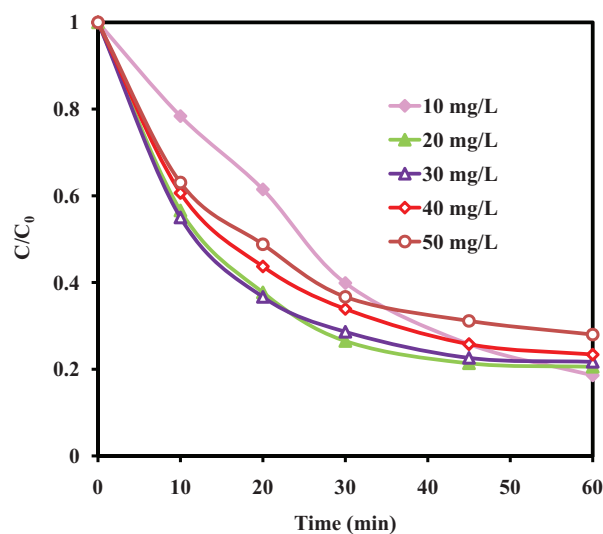

Fig. 7. Effect of initial bentazon concentration on the degradation of bentazon by the COP (pH = 7 and dosage = 0.5 g/L).

Table 2
Kinetics models, electrical energy per order equations, and parameters for the catalytic ozonation of bentazon

Kinetic models	Electrical energy per order	Parameters
Zero order $[\text{Bentazon}]_0 - [\text{Bentazon}]_t = k_0 t$	$E_{EO} = \dfrac{38.4 \times P}{V \times k_{obs}}$	$[\text{Bentazon}]_0$ (mg/L), $[\text{Bentazon}]_t$ (mg/L) k_0 (mol/L min), k_{obs} (min^{-1})
First order $\ln\dfrac{[\text{Bentazon}]_0}{[\text{Bentazon}]_t} = k_{obs} t$	$E_{EO} = \dfrac{p \times t \times 1000}{V \times 60 \times \log\dfrac{\text{Bentazon}_i}{\text{Bentazon}_f}}$	k_2 (L/mol min), t (min), k_c (mg/L min), K_{Bentazon} (L/mg), P (kW), V (L), E_{Eo} (kWh/m^3)
Second order $\dfrac{1}{[\text{Bentazon}]_t} \dfrac{1}{[\text{Bentazon}]_0} = k_2 t$		
Langmuir–Hinshelwood $\dfrac{d[\text{Bentazon}]}{dt} = \dfrac{k_c K_{\text{Bentazon}}[\text{Bentazon}]}{1 + K_{\text{Bentazon}}[\text{Bentazon}]_0} = k_{obs}[\text{Bentazon}]$ $\dfrac{1}{k_{obs}} = \dfrac{1}{k_c K_{\text{Bentazon}}} + \dfrac{[\text{Bentazon}]_0}{k_c}$		

Table 3
Kinetic parameters for the catalytic ozonation of bentazon at different initial Bentazon concentrations (ZnO-scallop shell dosage = 0.5 g/L and pH = 7)

[bentazon] (mg/L)	Zero order			First order			Second order	
	k_0 (mol/L min)	R^2	k_{obs} min^{-1}	$1/k_{obs}$ min	R^2	E_{EO} (kWh/m^3)	k_2 (L/mol min)	R^2
10	0.1402	0.8343	0.0307	32.573	0.9276	87.557	0.008	0.9626
20	0.2393	0.785	0.0266	37.893	0.9007	101.0526	0.0035	0.9594
30	0.3539	0.7722	0.0262	38.167	0.8889	102.5954	0.0023	0.9604
40	0.4741	0.8236	0.0247	40.485	0.9315	108.8259	0.0015	0.987
50	0.5609	0.8328	0.0217	46.082	0.9221	123.871	0.0009	0.9762

Table 4
Kinetic parameters for the catalytic ozonation of bentazon at different initial pHs (ZnO-scallop shell dosage = 0.5 g/L, $[\text{bentazon}]_0 = 7$)

pH	Zero order		First order		Second order	
	k_0 (mol/L min)	R^2	k_{obs} min^{-1}	R^2	k_2	R^2 (L/mol min)
3	0.2313	0.6852	0.0165	07976	0.0013	0.8745
5	0.2443	0.6223	0.0165	0.7809	0.0012	0.899
7	0.3539	0.7722	0.0262	0.889	0.0023	0.9604
9	0.2591	0.7986	0.022	0.9286	0.0021	0.9797
11	0.3009	0.6751	0.1024	0.1224	0.0014	0.9855

initial concentrations and pH values, respectively. The results of the kinetic studies showed that the second-order model was more suitable for explaining this process; other researchers have reported similar findings [46]. With increasing the initial concentration (10–50 mg/L), the rate of reaction of the second order (k_2) decreased (0.008–0.0009 L/mol min). K_{bentazon} and k_c were 19.2621 (L/mg) and 3.158 (mg/L min), respectively. Table 3 shows that the value of E_{EO} increased from 87.557 to 123.871 kWh/m^3 by increasing the initial concentration (10–50 mg/L). Also, the E_{EO} values for the ozone/ZnO-scallop

shell, ozone/scallop shell, ozone/ZnO and ozone processes were 102.595, 150.167, 253.585 and 340.253 kWh/m^3, respectively. The definitions of E_{EO}, k_2, K_{bentazon} and k_c have been presented in the study by Gholami et al. [8].
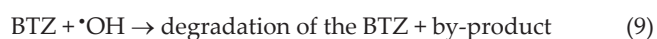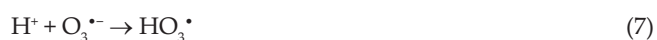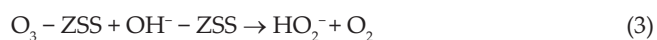
3.2.5. Effect of different purging gases

Fig. 8 indicates the effect of oxygen and nitrogen gas on the degradation of bentazon by the COP, under the following conditions: initial pH 7, catalyst dosage 0.5 g/L, initial

bentazon concentration 30 mg/L, gas flow rate 2 L/min and contact time 10–60 min. The decomposition of bentazon by the COP in the presence of oxygen and nitrogen gases increased from 27.48% to 52.63% and 41.97% to 71.78% with an increasing in reaction time from 10 to 60 min, respectively. Generally, the decomposition of bentazon in the presence of oxygen and nitrogen gases was lower than the ambient conditions. In many studies, dissolved oxygen and nitrogen gas were introduced as an electron scavenger and superoxide radical scavenger, respectively [26,47].

Hydroxyl radicals are formed according to Eqs. (1)–(8) [48] and degradation occurs based on Eq. (9). These radicals are not likely to be produced in the presence of electron and superoxide radical scavengers; consequently, in the presence of these two gases, the removal efficiency goes down.

$$BTZ + ZSS \rightarrow BTZ - ZSS \tag{1}$$

$$O_3 + ZSS \rightarrow O_3 - ZSS \tag{2}$$

$$O_3 - ZSS + OH^- - ZSS \rightarrow HO_2^- + O_2 \tag{3}$$

$$O_3 + HO_2^- \rightarrow O_3^{\bullet-} + HO_2^{\bullet} \tag{4}$$

$$HO_2^{\bullet} \rightarrow H^+ + O_2^{\bullet-} \tag{5}$$

$$O_3 + O_2^{\bullet-} \rightarrow O_3^{\bullet-} + O_2 \tag{6}$$

$$H^+ + O_3^{\bullet-} \rightarrow HO_3^{\bullet} \tag{7}$$

$$HO_3^{\bullet} \rightarrow O_2 + OH^{\bullet} \tag{8}$$

$$BTZ + {}^{\bullet}OH \rightarrow \text{degradation of the BTZ} + \text{by-product} \tag{9}$$

where, BTZ and ZSS depict bentazon and the ZnO-scallop shell catalyst, respectively.

3.2.6. Effect of the hydrogen peroxide

The effect of adding hydrogen peroxide on the decomposition of bentazon by the COP was measured under the following conditions: hydrogen peroxide concentration (2–50 mM), initial bentazon concentration (30 mg/L), catalyst dosage (0.5 g/L) and initial pH (7) for 60 min. When the concentration of H_2O_2 was raised from 2 to 50 mM, the decomposition efficiency increased from 77.52% to 90.47% (see Fig. 9), while the efficiency without using hydrogen peroxide was 76.86%. Hydroxyl radicals are produced from ozone reaction with hydrogen peroxide [49], and this leads to an increase in the degradation rate . In the study by Mortazavi et al., the removal efficiency of TOC by the COP in the presence of hydrogen peroxide was more than the removal efficiency by the COP alone [50]. The results reported in both studies by Mortazavi et al. and the current research showed that the removal efficiency by the COP in the presence of H_2O_2 was more than that by the COP without using H_2O_2.

3.2.7. Effect of the organic compounds

In the present work, the effect of humic acid, oxalic acid, EDTA, phenol, folic acid and citric acid (30 mg/L) on the decomposition of bentazon by the COP was investigated under the following conditions: initial pH = 7, catalyst dosage = 0.5 g/L and initial bentazon concentration = 30 mg/L within 60 min (Fig. 10). The addition of organic compounds decreased the removal efficiency. Generally, organic compounds are adsorbed into the active catalyst sites through competitive adsorption, thereby decreasing the degradation efficiency [8]. Also, folic acid as a superoxide scavenger and humic acid as a reactive oxygen species (ROS) scavenger can reduce the efficiency removal of bentazon in this process [51,52].

3.2.8. The comparison of each process and the mechanism of the reaction

In order to investigate the effects of different processes on the bentazon degradation, the performances of scallop
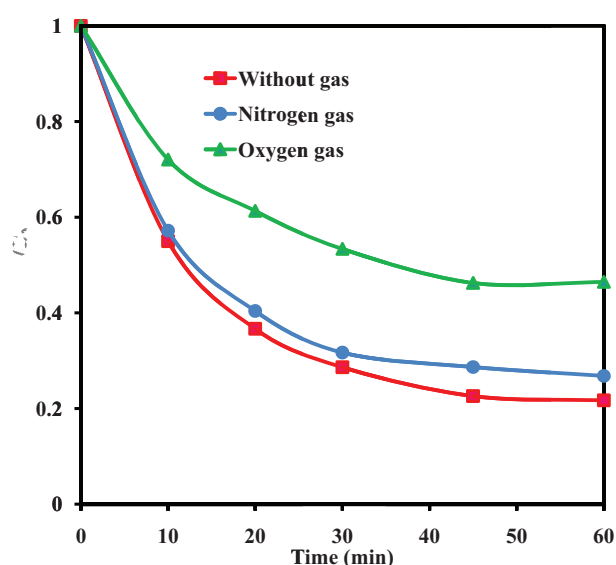
Fig. 8. Effect of different gas on the degradation of bentazon by the COP (pH = 7, dosage = 0.5 g/L and bentazon concentration = 30 mg/L).
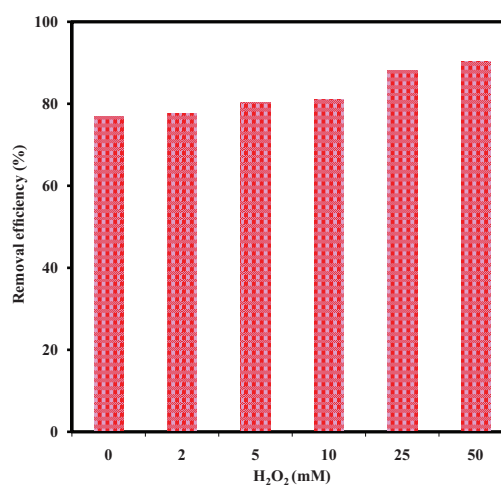
Fig. 9. Effect of hydrogen peroxide concentration on the degradation of bentazon by the COP (pH = 7, dosage = 0.5 g/L and bentazon concentration = 30 mg/L).
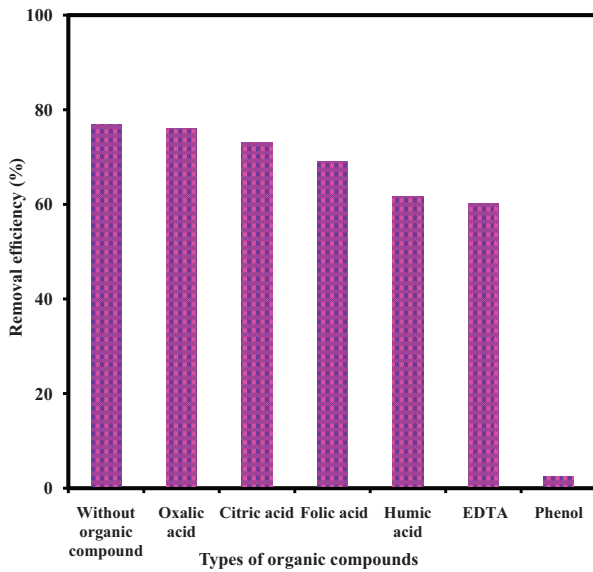
Fig. 10. Effect of organic compounds on the degradation of bentazon by the COP (pH = 7, dosage = 0.5 g/L, bentazon concentration = 30 mg/L and organic compounds = 30 mg/L).
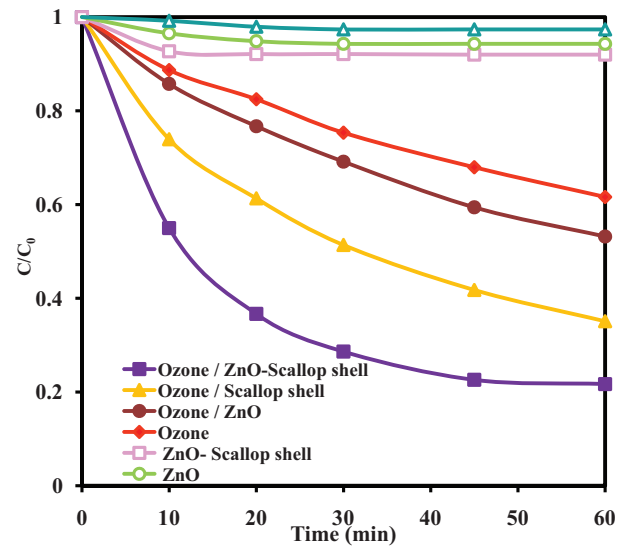

Fig. 11. Contribution of each process involved in the degradation of bentazon by the COP (pH = 7, dosage = 0.5 g/L and bentazon concentration = 30 mg/L).

shell, ZnO, ZnO-scallop shell, ozone, ozone-ZnO, ozone/scallop shell and ozone/ZnO-scallop shell were measured in the same reaction conditions as follows: initial pH = 7, catalyst dosage = 0.5 g/L, bentazon concentration = 30 mg/L and contact time = 10–60 min. The removal efficiencies for the mentioned processes above were 2.59%, 5.60%, 7.86%, 37.67%, 45.88%, 63.61% and 76.86%, respectively, (Fig. 11). In the study by Gholami et al. [8], the removal of bentazon using zinc oxide was 9%, which accords with our study's observation. In this study, the adsorption of bentazon by the scallop shell, ZnO and ZnO-scallop shell processes was very low, and the maximum efficiency was for ozone/ZnO-scallop shell (76.86%). This result indicates the ability of the COP for the elimination of bentazon in less time with a suitable efficiency. Moreover, the ZnO-scallop shell nanocomposite is a cheap and environmentally friendly catalyst. Also, in this process, ozone was used less.

In this study, to investigate the role of hydroxyl radicals in the degradation of bentazon by the COP, methanol was used as a scavenger to remove OH$^\bullet$. Fig. 12 shows the effect of methanol (10 mM) on the degradation of bentazon by the COP, under the following conditions: initial pH = 7, catalyst dosage = 0.5 g/L and initial bentazon concentration = 30 mg/L for different contact times 10–60 min. The removal of bentazon in the presence of methanol reached 60.76% after 60 min; this illustrates that hydroxyl radicals alone did not play a major role in the degradation. Therefore, hydroxyl radicals alongside other mechanisms and radicals caused the degradation of bentazon. Based on the pH results, these mechanisms and radicals include direct and indirect oxidation. Hence, both direct and indirect oxidation are effective in degradation of bentazon [Eqs. (10)-(11)]:

$$BTZ + ZSS \rightarrow BTZ - ZSS \tag{10}$$

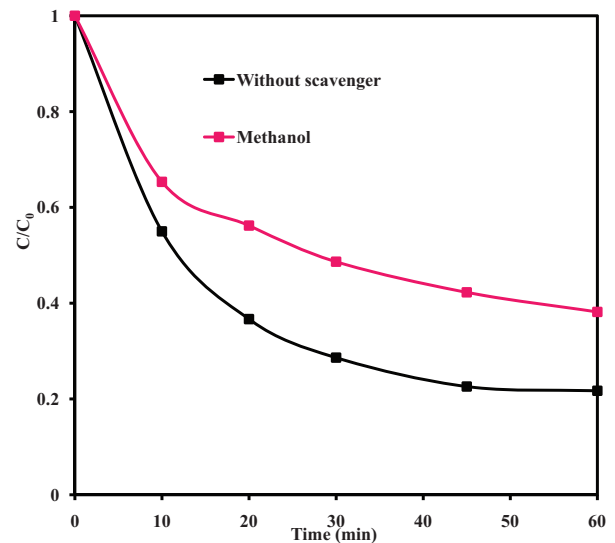$$O_3 + BTZ - ZSS \rightarrow BTZ \text{ degradation} + \text{by-product} \tag{11}$$

Fig. 12. Effect of hydroxyl radical scavenger (methanol = 10 mM) on degradation of bentazon by the COP (pH = 7, dosage = 0.5 g/L and bentazon concentration = 30 mg/L).

3.2.9. Removal of bentazon from real water

So as to study the ability of the ozone/ZnO-scallop shell process in the removal of bentazon from drinking water (real water), a sample of water was collected from drinking water in Rasht, Iran; then, 30 mg/L of bentazon and 0.5 g/L of ZnO-scallop shell were added to the water sample. Next, up to 60 min, the percentage of bentazon removal was calculated. As shown in Fig. 13, the removal efficiency of bentazon by the COP from drinking water was 70%, which was very close to the removal efficiency of bentazon from the synthetic water. Table 5 shows the characteristics of the real water; as shown in this table, the real water contains materials such as bicarbonate, chloride, sulfate and nitrate. This material with
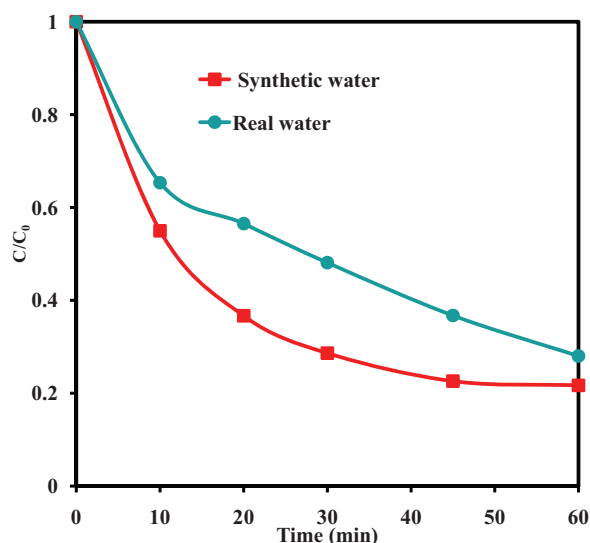
Fig. 13. Effect of the COP on bentazon removal from the real water (pH = 7, dosage = 0.5 g/L and bentazon concentration = 30 mg/L).

Table 5
Characteristics of the real water of Rasht, Iran

Parameters	Value
pH	7.8
Sulfate concentration (mg/L SO_4^{2-})	190.5
Chloride concentration (mg/L Cl^-)	202
Specific conductivity (mS/cm)	0.91
Total hardness (mg/L$CaCO_3^-$)	297
Calcium hardness (mg/L$CaCO_3^-$)	190
Carbonate hardness (mg/L$CaCO_3^-$)	98
Nitrate concentration (mg/L NO_3^-)	33.2
Nitrite concentration (mg l/L NO_2^-)	0
Total dissolved solids (TDS) (mg/L)	775

sitting on active catalyst sites can lead to the closure of these sites. As a result, catalyst activity is reduced and, in turn, the removal efficiency of bentazon is reduced [26].

3.2.10. Identification of reaction pathways of bentazon and mineralization of bentazon in the COP

Probable degradation pathways of bentazon during the COP, at initial pH = 7, catalyst dosage = 0.5 g/L and initial bentazon concentration = 30 mg/L for 60 min, were identified by GC–MS. Fig. 14 shows the bentazon decomposition pathways. 2-Amino-N-isopropyl-benzamide is created by the desulfuration of bentazon and then by adding hydroxyl radicals to bentazon and the loss of bentazon isopropyl amine, 2-amino benzoic acid is formed; in the next step, the oxidation of amino groups in 2-amino-N-isopropyl benzamide leads to the production of hydroxyamino-N-isopropyl-benzamide. The degradation pathways of bentazon in this study partly agree with the study by Mir et al [9]. The reason for the lack of complete agreement in the pathways of bentazon degradation in these two studies is that in the study by Mir et al. [9] the removal efficiency of bentazon was 100%, but in this study, it was 76.86%.

In order to investigate the mineralization rate of bentazon by the different processes, the performances of ozone, ozone-ZnO, ozone/scallop shell, ozone/ZnO-scallop shell, ozone/ZnO-scallop shell-N_2, ozone/ZnO-scallop shell-O_2 and ozone/ZnO-scallop shell-H_2O_2 were measured in the same reaction conditions. The removal efficiencies for the mentioned processes above were 34.67%, 45.88%, 63.61%, 76.86%, 71.78%, 52.63% and 90.47%, respectively. Also, the mineralization rates for the mentioned processes above were 19.85%, 28.36%, 49.32%, 55.56%, 48.69%, 51.23%, 85.69%, respectively. The mineralization rate of bentazon by the COP (in the conditions mentioned for the reaction pathways), was 55.56%. The concentrations of TOC before and after degradation of bentazon by the COP were 110.3 and 49.01 mg/L, respectively. In general, the mineralization rate in this study was similar to that of some catalytic ozonation
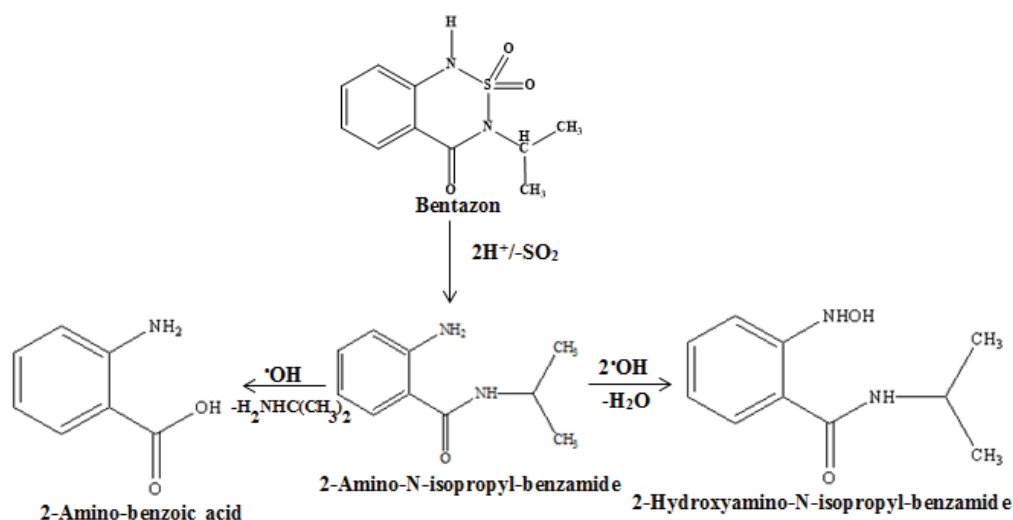

Fig. 14. Probable degradation pathways of bentazon during the COP (pH = 7, dosage = 0.5 g/L and bentazon concentration = 30 mg/L).

studies [53]. In some studies, the rate of mineralization of bentazon was very low relative to the removal efficiency of bentazon [13]; this difference indicates that most of bentazon had been decomposed to by-products, but, in this study, the mineralization rate (55.56%) was acceptable relative to the removal efficiency (76.86%).

4. Conclusion

In this study, by pH_{pzc}, XRD, FTIR, SEM and EDX characterization of the catalyst were studied, and results showed that the ZnO-scallop shell nanocomposite had been properly synthesized. The removal of bentazon in ozone/ZnO-scallop shell process was more than that of the ozone, ZnO, scallop shell, ZnO/ozone, ozone/scallop shell and ZnO-scallop shell processes. In addition, when hydrogen peroxide was added to the ozone/ZnO-scallop shell process, the removal efficiency increased. And, in the presence of organic compounds, lower bentazon was degraded. The degradation mechanism in this study was based on direct and indirect oxidation. Also, under the optimum conditions, the removal efficiency of bentazon from drinking water and mineralization rate of bentazon from synthetic water were 70% and 55.56%, respectively.

Acknowledgment

References

[1] N. Daneshvar, D. Salari, A. Niaei, A. Khataee, Photocatalytic degradation of the herbicide erioglaucine in the presence of nanosized titanium dioxide: comparison and modeling of reaction kinetics, J. Environ. Sci. Health, Part B, 41 (2006) 1273–1290.

[2] R. Pourata, A. Khataee, S. Aber, N. Daneshvar, Removal of the herbicide Bentazon from contaminated water in the presence of synthesized nanocrystalline TiO$_2$ powders under irradiation of UV-C light, Desalination, 249 (2009) 301–307.

[3] A. Derylo-Marczewska, M. Blachnio, A. Marczewski, A. Swiatkowski, B. Tarasiuk, Adsorption of selected herbicides from aqueous solutions on activated carbon, J. Therm. Anal. Calorim., 101 (2010) 785–794.

[4] World Health Organization (WHO), WHO Guidelines for Drinking Water Quality, World Health Organization, Geneva, 2004, p. 311.

[5] V. Njoku, M.A. Islam, M. Asif, B. Hameed, Utilization of sky fruit husk agricultural waste to produce high quality activated carbon for the herbicide bentazon adsorption, Chem. Eng. J., 251 (2014) 183–191.

[6] A. Omri, A. Wali, M. Benzina, Adsorption of bentazon on activated carbon prepared from *Lawsonia inermis* wood: equilibrium, kinetic and thermodynamic studies, Arab. J. Chem., 9 (2016) 1729–1739.

[7] M. Shirzad-Siboni, A. Khataee, A. Hassani, S. Karaca, Preparation, characterization and application of a CTAB-modified nanoclay for the adsorption of an herbicide from aqueous solutions: kinetic and equilibrium studies, C.R. Chim., 18 (2015) 204–214.

[8] M. Gholami, M. Shirzad-Siboni, M. Farzadkia, J.-K. Yang, Synthesis, characterization, and application of ZnO/TiO$_2$ nanocomposite for photocatalysis of a herbicide (Bentazon), Desal. Wat. Treat., 57 (2016) 13632–13644.

[9] N.A. Mir, M. Haque, A. Khan, M. Muneer, S. Vijayalakshmi, Photocatalytic degradation of herbicide Bentazone in aqueous suspension of TiO$_2$: mineralization, identification of intermediates and reaction pathways, Environ. Technol., 35 (2014) 407–415.

[10] S.D. Lambert, N.J. Graham, B.T. Croll, Degradation of selected herbicides in a lowland surface water by ozone and ozone-hydrogen peroxide, Ozone Sci. Eng., 18 (1996) 251–269.

[11] A.K. Abdessalem, N. Bellakhal, N. Oturan, M. Dachraoui, M.A. Oturan, Treatment of a mixture of three pesticides by photo- and electro-Fenton processes, Desalination, 250 (2010) 450–455.

[12] M. Peydayesh, P. Kazemi, A. Bandegi, T. Mohammadi, O. Bakhtiari, Treatment of bentazon herbicide solutions by vacuum membrane distillation, J. Water Process Eng., 8 (2015) 17–22.

[13] X. Wei, N. Gao, C. Li, Y. Deng, S. Zhou, L. Li, Zero-valent iron (ZVI) activation of persulfate (PS) for oxidation of bentazon in water, Chem. Eng. J., 285 (2016) 660–670.

[14] N. Daneshvar, A. Khataee, Removal of azo dye CI Acid Red 14 from contaminated water using Fenton, UV/H$_2$O$_2$, UV/H$_2$O$_2$/Fe (II), UV/H$_2$O$_2$/Fe (III) and UV/H$_2$O$_2$/Fe(III)/oxalate processes: a comparative study, J. Environ. Sci. Health, Part A Toxic/Hazard. Subst. Environ. Eng., 41 (2006) 315–328.

[15] A. Fujishima, T.N. Rao, D.A. Tryk, Titanium dioxide photocatalysis, J. Photochem. Photobiol., C, 1 (2000) 1–21.

[16] G. Moussavi, R. Khosravi, Preparation and characterization of a biochar from pistachio hull biomass and its catalytic potential for ozonation of water recalcitrant contaminants, Bioresour. Technol., 119 (2012) 66–71.

[17] A. Lv, C. Hu, Y. Nie, J. Qu, Catalytic ozonation of toxic pollutants over magnetic cobalt and manganese co-doped γ-Fe$_2$O$_3$, Appl. Catal., B, 100 (2010) 62–67.

[18] L. Yang, C. Hu, Y. Nie, J. Qu, Surface acidity and reactivity of β-FeOOH/Al$_2$O$_3$ for pharmaceuticals degradation with ozone: in situ ATR-FTIR studies, Appl. Catal. B, 97 (2010) 340–346.

[19] R. Darvishi Cheshmeh Soltani, A. Rezaee, A. Khataee, Combination of carbon black–ZnO/UV process with an electrochemical process equipped with a carbon black–PTFE-coated gas-diffusion cathode for removal of a textile dye, Ind. Eng. Chem. Res., 52 (2013) 14133–14142.

[20] P. Labhane, V. Huse, L. Patle, A. Chaudhari, G. Sonawane, Synthesis of Cu doped ZnO nanoparticles: crystallographic, optical, FTIR, morphological and photocatalytic study, J. Mater. Sci. Chem. Eng., 3 (2015) 39.

[21] N. Salah, A. Hameed, M. Aslam, S.S. Babkair, F. Bahabri, Photocatalytic activity of V doped ZnO nanoparticles thin films for the removal of 2-chlorophenol from the aquatic environment under natural sunlight exposure, J. Environ. Manage., 177 (2016) 53–64.

[22] M. Shirzad-Siboni, A. Khataee, S.W. Joo, Kinetics and equilibrium studies of removal of an azo dye from aqueous solution by adsorption onto scallop, J. Ind. Eng. Chem., 20 (2014) 610–615.

[23] T. Kawano, H. Imai, A simple preparation technique for shape-controlled zinc oxide nanoparticles: formation of narrow size-distributed nanorods using seeds in aqueous solutions, Colloids Surf., A, 319 (2008) 130–135.

[24] M. Shirzad-Siboni, M. Samarghandi, J.-K. Yang, S.-M. Lee, Photocatalytic removal of reactive black-5 dye from aqueous solution by UV irradiation in aqueous TiO$_2$: equilibrium and kinetics study, J. Adv. Oxid. Technol., 14 (2011) 302–307.

[25] M. Shirzad-Siboni, M. Farrokhi, R. Darvishi Cheshmeh Soltani, A. Khataee, S. Tajassosi, Photocatalytic reduction of hexavalent chromium over ZnO nanorods immobilized on kaolin, Ind. Eng. Chem. Res., 53 (2014) 1079–1087.

[26] A. Mohagheghian, K. Ayagh, K. Godini, M. Shirzad-Siboni, Photocatalytic reduction of Cr(VI) from synthetic, real drinking waters and electroplating wastewater by synthesized amino-functionalized Fe$_3$O$_4$–WO$_3$ nanoparticles by visible light, J. Ind. Eng. Chem., 59 (2018) 169–183.

[27] APHA, AWWA, WEF, Standard Methods for the Examination of Water and Wastewater, 20th ed., American Public Health Association, Washington, D.C., USA, 2000.

[28] A. Jonidi-Jafari, M. Gholami, M. Farzadkia, A. Esrafili, M. Shirzad-Siboni, Application of Ni-doped ZnO nanorods for degradation of diazinon: kinetics and by-products, Sep. Sci. Technol., 52 (2017) 2395–2406.

[29] N. Daneshvar, S. Aber, M.S. Seyed Dorraji, A.R. Khataee, M.H. Rasoulifard, Photocatalytic degradation of the insecticide diazinon in the presence of prepared nanocrystalline ZnO powders under irradiation of UV-C light, Sep. Purif. Technol., 58 (2007) 91–98.

[30] J.R. Abernathy, L.M. Wax, Bentazon mobility and adsorption in twelve Illinois soils, Weed Sci., 21 (1973) 224–227.

[31] T.E. Agustina, H.M. Ang, V.K. Vareek, A review of synergistic effect of photocatalysis and ozonation on wastewater treatment, J. Photochem. Photobiol., C, 6 (2005) 264–273.

[32] S.G. De Moraes, R.S. Freire, N. Duran, Degradation and toxicity reduction of textile effluent by combined photocatalytic and ozonation processes, Chemosphere, 40 (2000) 369–373.

[33] A. Alvares, C. Diaper, S. Parsons, Partial oxidation by ozone to remove recalcitrance from wastewaters – a review, Environ. Technol., 22 (2001) 409–427.

[34] G.G. Bessegato, J.C. Cardoso, B.F. da Silva, M.V.B. Zanoni, Combination of photoelectrocatalysis and ozonation: a novel and powerful approach applied in Acid Yellow 1 mineralization, Appl. Catal., B, 180 (2016) 161–168.

[35] F. Qi, W. Chu, B. Xu, Ozonation of phenacetin in associated with a magnetic catalyst $CuFe_2O_4$: the reaction and transformation, Chem. Eng. J., 262 (2015) 552–562.

[36] U. Von Gunten, Ozonation of drinking water: Part I. Oxidation kinetics and product formation, Water Res., 37 (2003) 1443–1467.

[37] B. Xu, F. Qi, J. Zhang, H. Li, D. Sun, D. Robert, Z. Chen, Cobalt modified red mud catalytic ozonation for the degradation of bezafibrate in water: catalyst surface properties characterization and reaction mechanism, Chem. Eng. J., 284 (2016) 942–952.

[38] Y.D. Shahamat, M. Farzadkia, S. Nasseri, A.H. Mahvi, M. Gholami, A. Esrafili, Magnetic heterogeneous catalytic ozonation: a new removal method for phenol in industrial wastewater, J. Environ. Health Sci. Eng., 12 (2014) 50.

[39] A. Rahmani, F. Barjasteh Askari, S.M. Asgari Gh, Degradation of reactive red 198 dye by catalytic ozonation using pumice and copper coated pumice, Fresenius Environ. Bull., 21 (2012) 2810–2817.

[40] G. Moussavi, M. Mahmoudi, Degradation and biodegradability improvement of the reactive red 198 azo dye using catalytic ozonation with MgO nanocrystals, Chem. Eng. J., 152 (2009) 1–7.

[41] W. Li, X. Lu, K. Xu, J. Qu, Z. Qiang, Cerium incorporated MCM-48 (Ce-MCM-48) as a catalyst to inhibit bromate formation during ozonation of bromide-containing water: efficacy and mechanism, Water Res., 86 (2015) 2–8.

[42] S.H. Lin, C.H. Wang, Ozonation of phenolic wastewater in a gas-induced reactor with a fixed granular activated carbon bed, Ind. Eng. Chem. Res., 42 (2003) 1648–1653.

[43] S. Dobaradran, R. Nabizaeh, A. Mahvi, A. Mesdaghinia, K. Naddafi, M. Yunesian, N. Rastkari, S. Nazmara, Survey on degradation rates of trichloroethylene in aqueous solutions by ultrasound, Iran. J. Environ. Health Sci. Eng., 7 (2010) 307–312.

[44] S. Dobaradaran, H. Lutze, A.H. Mahvi, T.C. Schmidt, Transformation efficiency and formation of transformation products during photochemical degradation of TCE and PCE at micromolar concentrations, J. Environ. Health Sci. Eng., 12 (2014) 16.

[45] F. Erol, T.A. Özbelge, Catalytic ozonation with non-polar bonded alumina phases for treatment of aqueous dye solutions in a semi-batch reactor, Chem. Eng. J., 139 (2008) 272–283.

[46] C.A. Guzman-Perez, J. Soltan, J. Robertson, Kinetics of catalytic ozonation of atrazine in the presence of activated carbon, Sep. Purif. Technol., 79 (2011) 8–14.

[47] A. Kagkoura, T. Skaltsas, N. Tagmatarchis, Transition metal chalcogenides/graphene ensembles for light-induced energy applications, Chem. Eur. J., 23 (2017) 12967–12979.

[48] A. Khataee, T.S. Rad, M. Fathinia, The role of clinoptilolite nanosheets in catalytic ozonation process: insights into the degradation mechanism, kinetics and the toxicity, J. Taiwan Inst. Chem. Eng., 77 (2017) 205–215.

[49] J.H. Suh, M. Mohseni, A study on the relationship between biodegradability enhancement and oxidation of 1, 4-dioxane using ozone and hydrogen peroxide, Water Res., 38 (2004) 2596–2604.

[50] S. Mortazavi, G. Asgari, S. Hashemian, G. Moussavi, Degradation of humic acids through heterogeneous catalytic ozonation with bone charcoal, React. Kinet. Mech. Catal., 100 (2010) 471–485.

[51] N. Di Simone, P. Riccardi, N. Maggiano, A. Piacentani, M. D'Asta, A. Capelli, A. Caruso, Effect of folic acid on homocysteine-induced trophoblast apoptosis, Mol. Hum. Reprod., 10 (2004) 665–669.

[52] H. Ou, N. Gao, Y. Deng, H. Wang, H. Zhang, Inactivation and degradation of *Microcystis aeruginosa* by UV-C irradiation, Chemosphere, 85 (2011) 1192–1198.

[53] Y. Yang, H. Cao, P. Peng, H. Bo, Degradation and transformation of atrazine under catalyzed ozonation process with TiO_2 as catalyst, J. Hazard. Mater., 279 (2014) 444–451.